Metallophysics and Advanced Technologies
Металофіз. новітні технол.
Metallofiz. Noveishie Tekhnol.
2026, vol. 48, No. 8, pp. 865–888
https://doi.org/10.15407/mfint.48.08.0865
Reprints available directly from the publisher

© 2026 G. V. Kurdyumov Institute for Metal Physics,
National Academy of Sciences of Ukraine
Published by license under
the G. V. Kurdyumov Institute for Metal Physics–
N.A.S. of Ukraine Publishers imprint.
Printed in Ukraine.

PACS numbers: 43.35.+d, 61.72.Dd, 61.72.Ff, 61.72.Hh, 62.20.Qp, 81.20.Ev, 81.40.Ef

Microstructural and Phase Evolution of AISI 316 Stainless Steel Produced by Selective Laser Melting and Hot Rolling during Heat Treatment and Ultrasonic Impact Treatment

S. M. Voloshko[*], I. A. Vladymyrskyi[*], M. I. Anyakin[*], N. A. Shapovalova[*], M. M. Voron[*,**], and A. P. Burmak[*]

[*]*National Technical University of Ukraine 'Igor Sikorsky Kyiv Polytechnic Institute', 37 Beresteiskyi Ave., UA-03056 Kyiv, Ukraine*
[**]*Physico-Technological Institute of Metals and Alloys, N.A.S. of Ukraine, 34/1 Academician Vernadsky Blvd., UA-03142 Kyiv, Ukraine*

The effects of fabrication route, heat treatment, and ultrasonic impact treatment (UIT) on the microstructure, phase composition, microhardness, and residual stresses of AISI 316 stainless steel produced by selective laser melting (SLM) and hot rolling (HR) are investigated. The SLM material exhibits a fine cellular structure and higher austenite stability, manifested by a lower susceptibility to the deformation-induced $\gamma \rightarrow \alpha'$ martensitic transformation compared with the hot-rolled steel. Heat treatment promotes microstructural homogenization, residual-stress relaxation, and an increase in the γ-phase fraction. UIT induces intense plastic deformation, refinement of coherent scattering domains, and compressive residual stresses. The maximum microhardness reaches 7.6 GPa for the hot-rolled steel and 6.7 GPa for the SLM material. The stronger hardening of the hot-rolled steel is associated with its greater susceptibility to deformation-induced martensitic transformation. Prior heat treatment significantly affects the response to subsequent

Corresponding author: Svitlana Mykhaylivna Voloshko
E-mail: voloshkosvetlana13@gmail.com

Citation: S. M. Voloshko, I. A. Vladymyrskyi, M. I. Anyakin, N. A. Shapovalova, M. M. Voron, and A. P. Burmak, Microstructural and Phase Evolution of AISI 316 Stainless Steel Produced by Selective Laser Melting and Hot Rolling during Heat Treatment and Ultrasonic Impact Treatment, *Metallofiz. Noveishie Tekhnol.*, **48**, No. 8: 865–888 (2026). DOI: 10.15407/mfint.48.08.0865

© Publisher PH 'Akademperiodyka' of the NAS of Ukraine, 2026. This is an open access article under the CC BY-ND license (https://creativecommons.org/licenses/by-nd/4.0)

UIT, with annealing followed by UIT providing the largest and most stable increase in microhardness. The results demonstrate the effectiveness of combining heat treatment and UIT for controlling the structural and phase state and mechanical characteristics of AISI 316 stainless steel produced by different fabrication routes.

Key words: AISI 316, additive manufacturing, heat treatment, ultrasonic impact treatment, microstructure, phase composition, microhardness.

Досліджено вплив технології виготовлення, термічного оброблення й ультразвукового ударного оброблення (УЗУО) на мікроструктуру, фазовий склад, мікротвердість і рівень залишкових напружень неіржавійної криці AISI 316, одержаної методою селективного лазерного топлення (SLM) та гарячого вальцювання (HR). Матеріял, виготовлений методою SLM, характеризується дрібнодисперсною комірчастою структурою та вищою стабільністю аустенітної γ-фази, що проявляється у меншій схильності до деформаційно-індукованого мартенситного перетворення $\gamma \to \alpha'$ порівняно з гарячекатаною крицею. Термічне оброблення сприяє гомогенізації мікроструктури, релаксації залишкових напружень і збільшенню частки γ-фази. УЗУО забезпечує інтенсивну пластичну деформацію поверхневого шару, зменшення розміру областей когерентного розсіяння та формування стискальних напружень. Максимальна мікротвердість сягає 7,6 ГПа для гарячекатаної криці та 6,7 ГПа для матеріялу, одержаного методою SLM. Вища ефективність зміцнення гарячекатаної криці пов'язана з більшою схильністю її до деформаційно-індукованого мартенситного перетворення. Попереднє термічне оброблення істотно впливає на ефективність подальшого УЗУО, причому найбільше та найбільш стабільне підвищення мікротвердости забезпечує поєднання відпалу з УЗУО. Одержані результати підтверджують ефективність комплексного застосування термічного та поверхневого деформаційного оброблення для керування структурно-фазовим станом, мікротвердістю та залишковими напруженнями криці AISI 316, виготовленої різними технологічними методами.

Ключові слова: AISI 316, адитивне виробництво, термічне оброблення, ультразвукове ударне оброблення, мікроструктура, фазовий склад, мікротвердість.

(Received 3 July, 2026; in final version, 22 July, 2026)

1. INTRODUCTION

Austenitic stainless steels are important structural materials due to their high corrosion resistance, excellent processability and non-magnetic properties [1, 2]. Owing to their high deformability, these steels are used to produce vessels for the chemical, energy and food industries, pipes, capillaries and various complex-shaped components, including critical-purpose products [3].

The main grades of austenitic stainless steels include AISI 304, 306, 316 and 321. These steels are similar in chemical composition and me-

chanical properties, but differ in the alloying additions that determine their service performance. AISI 304, containing 18–20% wt. Cr and 8–11% wt. Ni, is the most widely used base grade in the chemical and food industries. A distinctive feature of AISI 316 is Cr content lower by ≅ 2% wt. and Ni content higher by ≅ 2% wt. together with 2–3% wt. Mo. This composition provides much higher corrosion resistance and a lower susceptibility to intergranular corrosion; therefore, grade 316 is often referred to as 'marine' or 'chemical' stainless steel. AISI 321 is close in composition to AISI 304; however, it contains Ti providing the highest heat resistance without loss of corrosion resistance. Owing to its high resistance at elevated temperatures and improved weldability, it is used for components of military equipment, including aviation parts, heat exchangers and related products [2, 4, 5].

As was already mentioned, these austenitic stainless steels reveal a similar set of mechanical properties. After quenching, their ultimate tensile strength is of 480–580 MPa, yield strength is of 200–250 MPa and elongation is of 35–55% [2, 5, 6]. These properties can be effectively modified by deformation and heat treatment. For example, cold plastic deformation promotes grain refinement, the development of crystallographic texture, and deformation-induced martensite formation, increasing the microhardness from 340 to 540 *HV*. Depending on the processing conditions, the resulting strength reaches 700–1600 MPa, while the elongation decreases to 2–20%, accompanied by deterioration in corrosion resistance [7, 8]. Multiple equal-channel angular pressing of AISI 316 steel refines the grain size to 10–40 nm and increases the yield strength to 1480 MPa; however, these improvements are achieved at the expense of high energy consumption [9]. By combining deformation and heat treatment, the microstructural parameters of austenitic stainless steels can be controlled effectively and their mechanical properties can be varied over a wide range [10].

Despite these advantages and the possibility of controlling structural properties, phase composition and mechanical characteristics, improvement of corrosion resistance remains a key issue for austenitic stainless steels. Various surface treatments of steel products are primarily used for this purpose. For example, in Ref. [11], the effect of laser surface treatment on the chemical composition, surface morphology and corrosion resistance of AISI 304, AISI 316 and AISI 321 steels was investigated. A decrease in the concentrations of Cr and Ni and an increase in O content at the surface were observed, resulting in different corrosion resistance at a certain depth from the surface. The most pronounced positive effect was obtained for AISI 321 owing to Ti migration towards the surface. However, the specimen surface remains continuous only after treatment with low laser energies. When the energy density exceeded 100 J/cm^2, cracks appear on the surface, significantly deteriorating corrosion resistance and fatigue strength. In con-

trast, deformation-induced surface nanostructuring combined with annealing led to Cr enrichment of the treated surface and, consequently, to a substantial improvement in corrosion resistance. Lei *et al.* showed [12] that a preformed gradient nanostructured (GNS) surface layer of 316L stainless steel was subjected to surface mechanical rolling treatment (SMRT) followed by annealing at 700°C. Tensile tests showed that the strength–ductility ratio is higher for the annealed SMRT material, while grain size and hardness of the GNS layer remain sufficiently stable. In addition, significant Cr enrichment was detected for the GNS surface layer after annealing, leading to a considerable corrosion resistance enhancement. In Ref. [13], a $\cong$ 20-μm thick nanostructured surface layer was formed on a low-carbon steel plate by surface mechanical attrition treatment (SMAT). In particular, the authors showed that after SMAT, a much thicker Cr diffusion layer was obtained compared to the coarse-grained specimen after chromizing, especially at low temperatures. For the SMAT material, the temperature of chromium-containing compound formation is considerably lower and the amount of chromium carbides is higher in comparison with its coarse-grained counterpart. Thus, surface mechanical attrition-assisted chromizing of austenitic stainless steels also improves corrosion resistance.

Other methods of surface alloying and strengthening of austenitic stainless steels were actively investigated in recent decades as well, including plasma surface alloying [14], electrolytic coating deposition [15], thermochemical treatment with simultaneous chromizing and nitrocarburizing [16], aluminosiliconizing [17] to name just a few. Austenitic stainless steels exhibit superior mechanical performance, characterized by high yield and tensile strength, good ductility, excellent fracture toughness, and enhanced fatigue and wear resistance, when the modified surface contains a fine-crystalline structure both in the base metal and in the coating phases. In particular, oxides, carbides or nitrides could simultaneously improve fatigue strength, corrosion resistance and wear resistance. However, it should be noted that, under sufficient mechanical loading, such surfaces might fail because of structural anisotropy.

A homogeneous fine-grained microstructure leading to higher corrosion resistance compared to rolled products can be achieved by additive manufacturing of austenitic stainless steel components [18, 19]. For example, wire-arc additive manufacturing (WAAM) of AISI 316L steel increases the material strength by 58% and the fatigue strength by 10% [20]. Alloy produced by selective laser melting (SLM) reveal a finer-grained structure with grain size of 1–5 μm and higher ultimate tensile and yield strengths of 650 MPa and 550 MPa, respectively, albeit with lower ductility compared with the same alloy manufactured by conventional routes such as forging and casting [21]. The reduced

ductility of SLM specimens is compensated by their higher strength.

Therefore, additively manufactured components made of austenitic stainless steels are promising for subsequent surface treatment due to fine-grained and homogeneous microstructure. Such treatment should not promote grain growth but should refine grains, thereby increasing surface hardness and, where possible, enrich the surface with interstitial elements improving the corrosion and wear resistance. Since SLM-fabricated 316L components reveal an anisotropic cellular structure with a high density of dislocations and macrodefects, surface or deformation treatment should be combined with thermal annealing [22].

Since printed components usually have complex geometries, the choice of post-processing approaches is limited. It should also be considered that prolonged exposure to high temperatures might be unfavourable for structural modification of additively produced specimens. So, additive manufacturing followed by heat treatment and subsequent ultrasonic impact treatment represents an effective processing route for producing austenitic stainless-steel components with a homogeneous microstructure and enhanced mechanical and service properties. The efficiency of this approach for surface grain refinement and strengthening was demonstrated for metallurgically produced AISI 321 steel [23]. Another successful example is the combination of recrystallization annealing at 900°C for 1 hour with ultrasonic surface modification of AISI 316 steel, which restore ductility while maintaining an increased surface microhardness of $\cong 400\ HV_{10}$ [24].

Thus, the aim of the present study is to perform a comparative analysis of the structural properties, phase characteristics and hardness changes of 316L steel produced by metallurgical and SLM routes after heat treatment, ultrasonic impact treatment and their combination.

2. MATERIALS AND METHODS

Specimens of AISI 316 austenitic stainless steel with the following chemical composition [% wt.] were used: Cr, 16–18, Ni, 10–14, Mo, 2–3, Mn ≤ 2, Si ≤ 1, Cu ≤ 0.75, Fe—balance. Materials produced by two routes were investigated: SLM and a conventional route (HR) involving melting, formation of rolled stock and production of deformed billets.

SLM specimens in the form of parallelepipeds (15 mm in length, 8 mm in width, and 6.5 mm in height) were fabricated using an Alfa-150D 3*D* printer manufactured by ALT. The printer was equipped with a 200 W ytterbium fibre laser operating at a wavelength of 1070 ± 2 nm, with a focused laser beam diameter of 45 μm. The scanning speed was 500 mm/s, the powder layer thickness was 25 μm, and the hatch spacing was 150 μm. Spherical AISI 316L austenitic stainless-steel powder with a particle size range of 15–53 μm was used. To minimize oxidation, the specimens were fabricated in an inert argon (Ar) atmos-

phere [25].

Specimens of deformed AISI 316 stainless steel were produced by a standard industrial metallurgical route. The starting components were melted in an electric arc furnace, followed by argon-oxygen decarburization refining to ensure the specified chemical composition in accordance with ASTM A240/A240M requirements for steel products in bar form. After refining, the metal was cast into semi-finished products, which were subsequently hot rolled and slowly cooled in air.

Both types of investigated specimens were subjected to heat treatment; the treatment conditions are given in Table 1 in accordance with ASTM A276.

AISI 316 stainless-steel specimens were subjected to ultrasonic impact treatment both in the as-received state and after thermal impact. The ultrasonic impact treatment (UIT) was carried out in air using a UZG-300 device equipped with an impact head containing a cylindrical 10×18 mm striker made of hardened AISI 52100 steel [26]. A single-contact normal impact-loading mode was used [27]. The amplitude at the concentrator end face was 25 μm, and the treatment duration was varied from 30 to 300 s. During loading, each specimen received 10^4–10^5 impacts.

Microstructural studies were performed using an iScope IS.1053-PLMi optical metallographic microscope. Microhardness was measured by the Vickers method using an LHVS-1000Z tester under a 100 g load and a dwell time of 10 s.

X-ray diffraction studies were carried out using a Rigaku Ultima IV diffractometer with radiation CuK_α: 2θ range—20–120°, step size of 0.04° and counting time 2 s per point. The PDXL software package and the ICDD international diffraction database (PDF-2, 2025) were used to analyse the XRD patterns, calculate the coherent scattering domain (CSD) size, lattice microstrain (ε) and perform quantitative phase analysis. The quantitative phase composition was calculated from the integrated intensities of non-overlapping diffraction peaks characteristic of each phase using Rietveld refinement in PDXL.

TABLE 1. Heat-treatment conditions for AISI 316 stainless steel.

	SLM alloy	
1	As-received state	SLM–0
2	Annealing at 1050 ± 10°C for 30 min followed by furnace cooling	SLM–T1
3	Annealing at 1050 ± 10°C for 30 min followed by water quenching	SLM–T2
	Deformed alloy (hot rolling)	
4	Initial state	HR–0
5	Annealing at 1050 ± 10°C for 30 min followed by furnace cooling	HR–T1
6	Annealing at 1050 ± 10°C for 30 min followed by water quenching	HR–T2

First-order residual stresses were determined by the $\sin^2\psi$ method from the change in the angular position of the γ-Fe(311) diffraction peak at $\psi = 0°$, $-10°$, $-20°$, $-30°$ and $-40°$. A Savitzky–Golay function was used to smooth the diffraction-peak profiles, and a Sonneveld–Vissers function was used for background separation. The angular positions of diffraction peaks were determined from the centre-of-gravity positions. The data were processed using Rigaku Residual Stress Analysis software.

3. RESULTS AND DISCUSSION

Figure 1 compares the microhardness and first-order residual-stress level of AISI 316 steel produced by two routes, SLM and HR, in the as-received state (0), after annealing (T1) and after water quenching (T2).

In the as-received state, the microhardness of the SLM and HR specimens is close with a value of ≅ 2.8–3.0 GPa (Fig. 1, *a*). This fact indicates a relatively high strengthening level of both studied materials, although the mechanisms responsible for their structure formation differ substantially.

After heat treatment, the microhardness of the SLM specimen slightly decreases and remains at about 2.5 GPa for both T1 and T2. By contrast, the microhardness of the hot-rolled specimens increases from 2.8 to approximately 3.0 GPa after HR–T1 annealing and to 3.5 GPa after T2 water quenching. This difference can be explained by the distinct microstructures of the two materials. In the as-built condition, the SLM material is characterized by a fine cellular-dendritic microstructure and residual stresses formed during rapid solidification

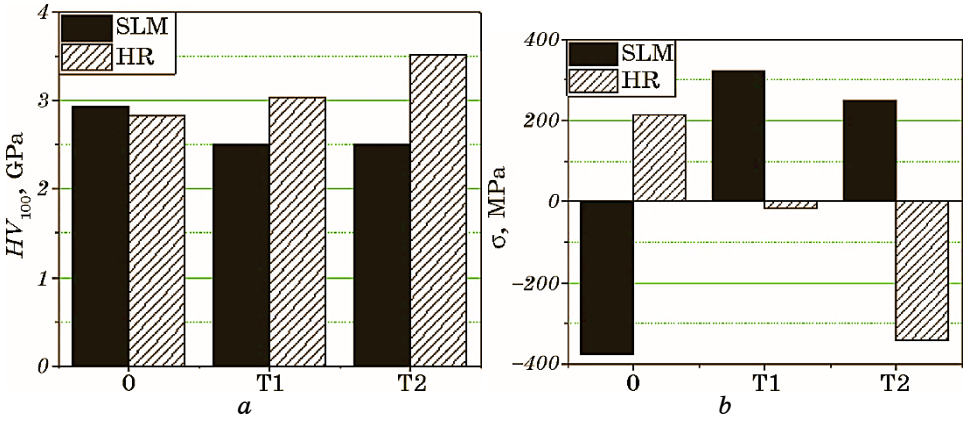


Fig. 1. Microhardness (*a*) and first-order residual stresses (*b*) in AISI 316 stainless steel produced by selective laser melting and hot rolling in the as-received state and after heat treatment.

(Fig. 1, *b*). Heat treatment partially relieves these residual stresses while preserving the refined microstructure, resulting in only a slight decrease in microhardness.

For the hot-rolled state, heat treatment may primarily promote recovery, stabilization of the subgrain structure and, depending on the heat-treatment temperature, recrystallization and precipitation of secondary phases, which increases microhardness. The increase in microhardness after annealing is attributed to the microstructural changes induced by heat treatment. Since the residual stresses are largely relieved after annealing (Fig. 1, *b*), the observed strengthening is likely associated with microstructural refinement rather than residual stress effects. In turn, water quenching preserves the recrystallized microstructure and introduces residual stresses that are subsequently transformed from tensile to compressive during ultrasonic impact treatment. Their magnitude nearly reaches the level typical for the as-received SLM material.

To identify the specific features of microstructural changes in SLM AISI 316 steel in more detail manner, comparison with the conventionally deformed material is required.

Figure 2, *a* shows that, in the as-received state, the SLM structure is characterized by pronounced anisotropy and elongated overlapping melt-pool tracks, which are typical for structure formation during additive manufacturing. The boundaries between individual melt tracks remain clearly visible, indicating the local nature of the thermal effect.

After annealing (Fig. 2, *c*), the microstructure becomes considerably more homogeneous, and the boundaries between individual melt pool regions become less distinct. The pronounced heterogeneity characteristic of the as-built condition is substantially reduced, while localized contrast-rich regions remain visible within the microstructure. These changes indicate significant microstructural evolution during annealing and are consistent with recovery and relaxation of residual stresses.

After water quenching (Fig. 2, *e*), the SLM specimens retain more features of the as-received structure, which is related to the shorter high-temperature exposure. The outlines of the melt pool regions become less visible, and the structure becomes more homogeneous while retaining its fine dispersion. The simultaneous substantial decrease in grain-boundary contrast also indicates the occurrence of polygonization.

Considering the simultaneous changes in microhardness and residual stresses, which will be discussed below, water quenching modifies the microstructural and stress state of the material. The XRD patterns reveal the coexistence of austenite γ-Fe and deformation-induced martensite α'-Fe, indicating a two-phase $\gamma + \alpha'$ structure. The relative intensities of the γ- and α'-phase reflections change with increasing UIT duration, reflecting the progressive $\gamma \rightarrow \alpha'$ deformation-induced mar-

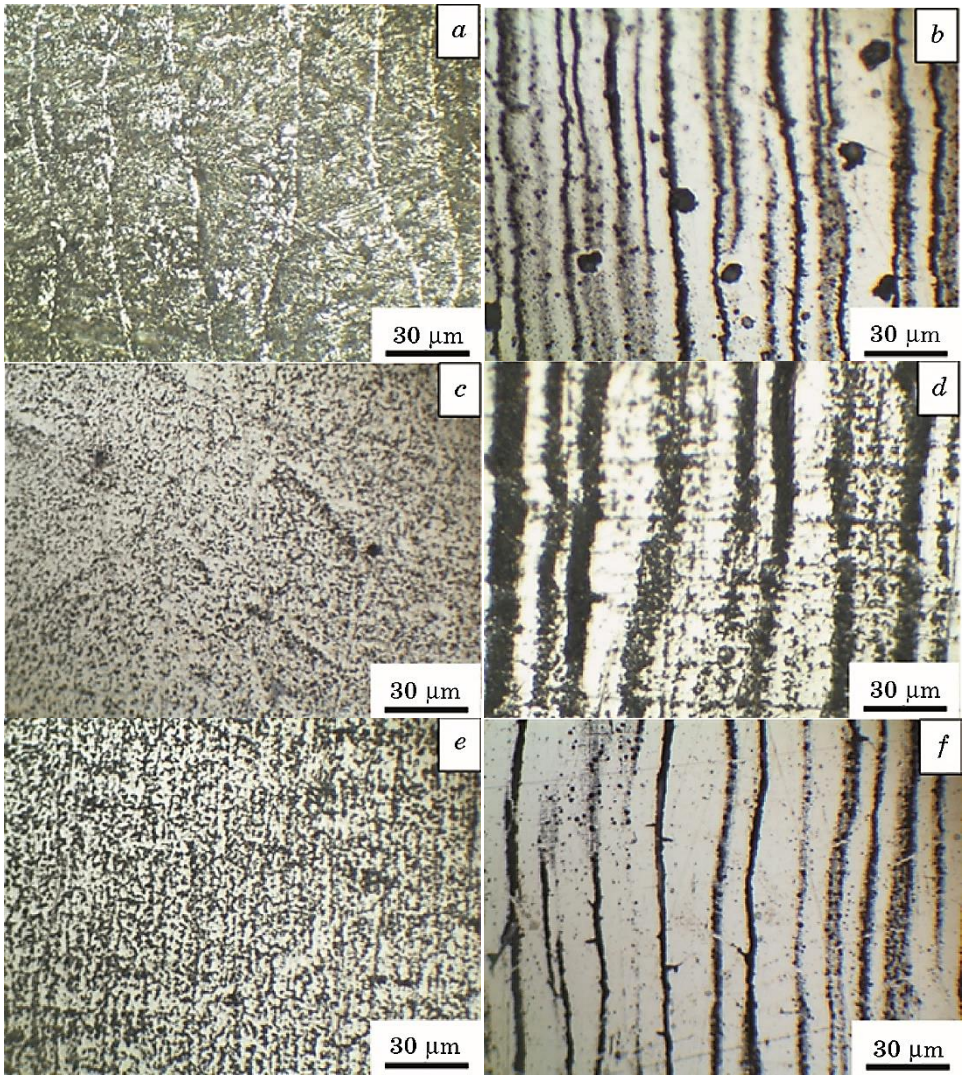


Fig. 2. Microstructure of AISI 316 stainless steel produced by selective laser melting (*a*, *c*, *e*) and hot rolling (*b*, *d*, *f*): as-received state (*a*, *b*), after annealing (*c*, *d*), after water quenching (*e*, *f*).

tensitic transformation. Therefore, the differences in residual stress and microhardness between the heat-treated conditions cannot be attributed solely to residual stress relaxation and are also related to changes in phase composition and microstructure.

The hot-rolled material in the as-received state (Fig. 2, *b*) exhibits a pronounced banded morphology, with elongated grains or structural regions oriented predominantly along the rolling direction. Distinct

dark contrast features are distributed within the elongated regions and locally concentrated near their boundaries.

After annealing (Fig. 2, *d*), the banded structure is largely retained, while the grains remain relatively intact and locally exhibit an increase in size. This is reflected by an approximately 1.5–2-fold increase in the apparent grain width, accompanied by changes in the morphology and continuity of the intergranular regions. The dispersed contrast features observed in the as-received condition become less pronounced after annealing, indicating significant microstructural evolution during heat treatment. The low level of residual stresses after annealing (Fig. 1, *b*) indicates substantial stress relaxation during the heat-treatment process.

After water quenching (Fig. 2, *f*), the microstructure of the AISI 316 stainless steel exhibits features intermediate between those observed in the as-received and annealed conditions. The heat treatment results in an increase in the apparent grain width and makes some grain boundaries more distinct, while regions with less distinct boundaries remain visible. The water-quenched condition is also characterized by a relatively high level of compressive residual stresses, comparable to that measured in the as-received SLM material (Fig. 1, *b*). The simultaneous increase in microhardness and development of compressive residual stresses indicate a pronounced change in the mechanical and stress state of the surface layer after water quenching.

Heat treatment promotes structural changes in both types of the investigated material; however, the effect varies to the different mechanisms of initial microstructure formation. In the SLM material, owing to the higher grain dispersion and the initially high level of compressive stresses, recrystallization processes, particularly grain-growth recrystallization, proceed more rapidly. In the hot-rolled material, these processes occur more slowly and are less pronounced due to the stable textured structure.

Figure 3 shows fragments of XRD spectra and the results of quantitative phase analysis of AISI 316 stainless steel produced by selective laser melting and hot rolling in the as-received state and after heat treatment.

In the as-received state (Fig. 3, *a*), the austenitic γ-phase predominates in the both cases. Its content is $\cong 99\%$ for the HR specimen and $\cong 93\%$ for the SLM specimen. The results indicate partial martensite formation during selective laser melting caused by the high thermal gradients and substantial internal stresses typical for additive manufacturing.

After annealing (Fig. 3, *b*), the SLM material exhibits a pronounced increase in the γ-austenite fraction, reaching approximately 98%. The XRD patterns show a dominant γ-Fe phase, while the contribution of the α'-Fe phase is substantially reduced after annealing. This phase re-

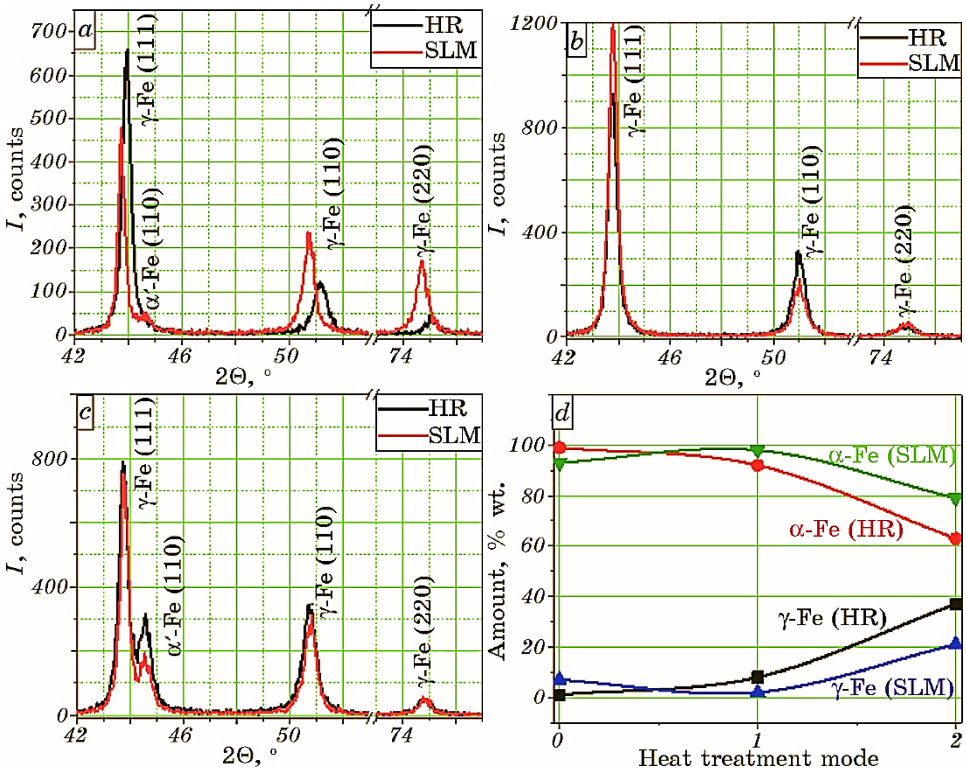


Fig. 3. XRD patterns of AISI 316 stainless steel produced by selective laser melting and hot rolling: as-received state (*a*), after annealing (*b*), after water quenching (*c*), and quantitative phase composition after different production and treatment routes (*d*).

distribution is accompanied by a reduction in residual stresses, indicating significant microstructural and stress-state changes during heat treatment. The γ-phase also predominates in the hot-rolled material after annealing.

The most significant phase composition modification occurs after water quenching (Fig. 3, *c*). In the both cases, the amount of α-phase increases while the fraction of austenite decreases accordingly. However, the rate of these changes strongly depends on the fabrication route. In the hot-rolled specimen, the α-phase fraction increases to 37%, whereas the γ-phase content decreases to 63%. In turn, for the SLM specimen, these changes are less pronounced: the α-phase content is of 21%, while the γ-phase fraction remains at 79%. This fact indicates higher stability of the austenitic structure in the material produced by selective laser melting.

Thus, substantial differences in the phase composition of AISI 316

steel depending on the fabrication route are achieved after the heat-treatment stage. The material produced by selective laser melting demonstrates higher stability of the austenitic phase and a lower tendency to phase transitions, whereas the hot-rolled steel is characterized by a higher α-phase fraction after heat treatment and higher sensitivity to subsequent deformation strengthening.

Since the phase composition, structural defectiveness and internal-stress level determine the response of the material to external deformation, the efficiency of ultrasonic impact treatment can also be expected to depend strongly on the structural state formed during heat treatment stage. Therefore, the next step of the study examined the effect of ultrasonic impact treatment and the combined effect of heat treatment and UIT on microhardness, surface morphology, phase composition, coherent scattering domain size and residual stresses of AISI 316 steel produced by selective laser melting and hot rolling.

Figure 4 shows the change in microhardness of AISI 316 steel after different treatment regimes.

All T0, T1 and T2 specimens exhibit a nonmonotonic change in microhardness with increasing UIT duration. For specimens not subjected to heat treatment (T0), the microhardness varies in an oscillatory manner with UIT time. For the SLM case, the hardness increases rapidly to a maximum of 6.5 GPa after 80 s, and then sharply decreases to 4.5 GPa at 120 s, with the following increase up to 6.4 GPa at 210 s and final decrease to 5 GPa. For the HR specimen (T0), strengthening occurs in two stages: up to 6.5 GPa after 60 s of UIT and up to 7.6 GPa after 120 s, followed by a sharp decrease in hardness to 4.5 GPa. This behaviour can be associated with efficient accumulation of crystal-lattice defects, refinement of structural features and formation of a

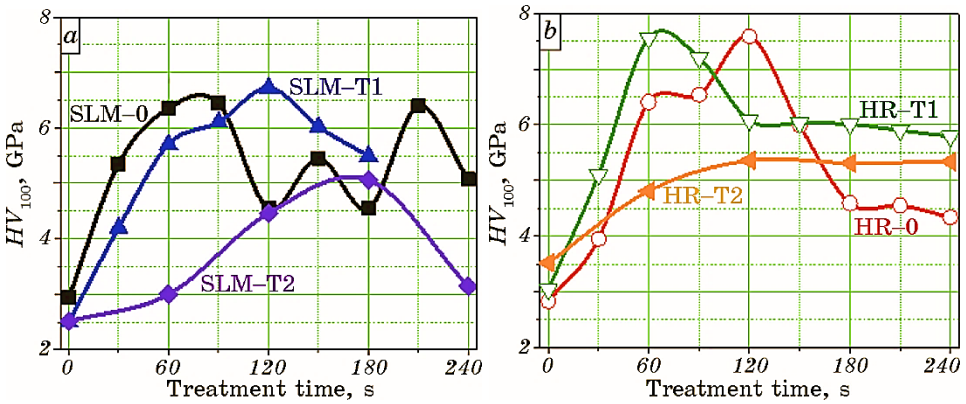


Fig. 4. Microhardness of AISI 316 stainless steel produced by selective laser melting (SLM, *a*), and hot rolling (HR, *b*) as a function of ultrasonic impact treatment duration.

strain-hardened surface layer at the initial stages of UIT, followed by the onset of relaxation processes.

After annealing according to the T1 and T2 regimes, the initial microhardness values of the SLM specimens decrease relative to the T0 state due to relaxation of internal stresses and partial structural recovery. At the following stage, UIT leads to significant increase in microhardness. For the SLM–T1 condition, the strengthening maximum is delayed compared to T0 and reaches 6.7 GPa after 120 s of the treatment, followed by a gradual decrease. The HR–T1 condition is potentially the most stable: the hardness rapidly increases to 7.6 GPa after only 60 s of the treatment and remains at a high level of 6.0–6.4 GPa up to 240 s.

After water quenching (T2), the microhardness behaviour differs depending on the production procedure. The SLM–T2 sample shows the poorest stability. Strengthening proceeds very slowly, reaching only 5.06 GPa at a UIT duration of 180 s, and decreases to 3.1 GPa at the final stage of the treatment (240 s), which is an indicator of complete annealing and recrystallization. The hot-rolled stainless steel (HR–T2) is characterized by a monotonic increase in microhardness already at the initial stages of UIT, with a maximum value of 5.3 GPa after 120 s, followed by stabilization at this.

Comparison of thermal and deformation effects on the microhardness of stainless steel produced by selective laser melting and hot rolling allows to found that the HR steel exceeds the SLM steel in maximum strengthening capacity: the maximum microhardness of HR material reaches 7.6 GPa (T0 and T1 conditions), while, for SLM, it does not exceed 6.7 GPa (T1 condition). The higher maximum microhardness of hot-rolled specimens, especially after annealing, associated with more effective strain hardening and formation of a finely dispersed substructure during UIT. In contrast, SLM specimens show a smaller increase in microhardness during UIT, caused by the specific cellular–dendritic structure and residual stresses formed during additive manufacturing.

Regarding the treatment duration required to achieve the maximum hardness, the hot-rolled steel (HR–T1) responds much faster, reaching its peak after 60 s of ultrasonic impact treatment, whereas the SLM–T1 specimen requires 120 s to attain a comparable strengthening effect. It can be concluded that for AISI 316 steel produced by both SLM and HR, annealing with a furnace cooling (T1) is considerably more effective for subsequent ultrasonic strengthening since it creates prerequisites for phase or dispersion strengthening. In contrast, water quenching (T2) makes the matrix excessively prone for rapid recrystallization during UIT.

Figure 5 demonstrates the effect of ultrasonic impact treatment (UIT) on the surface morphology of selective laser melted and hot-

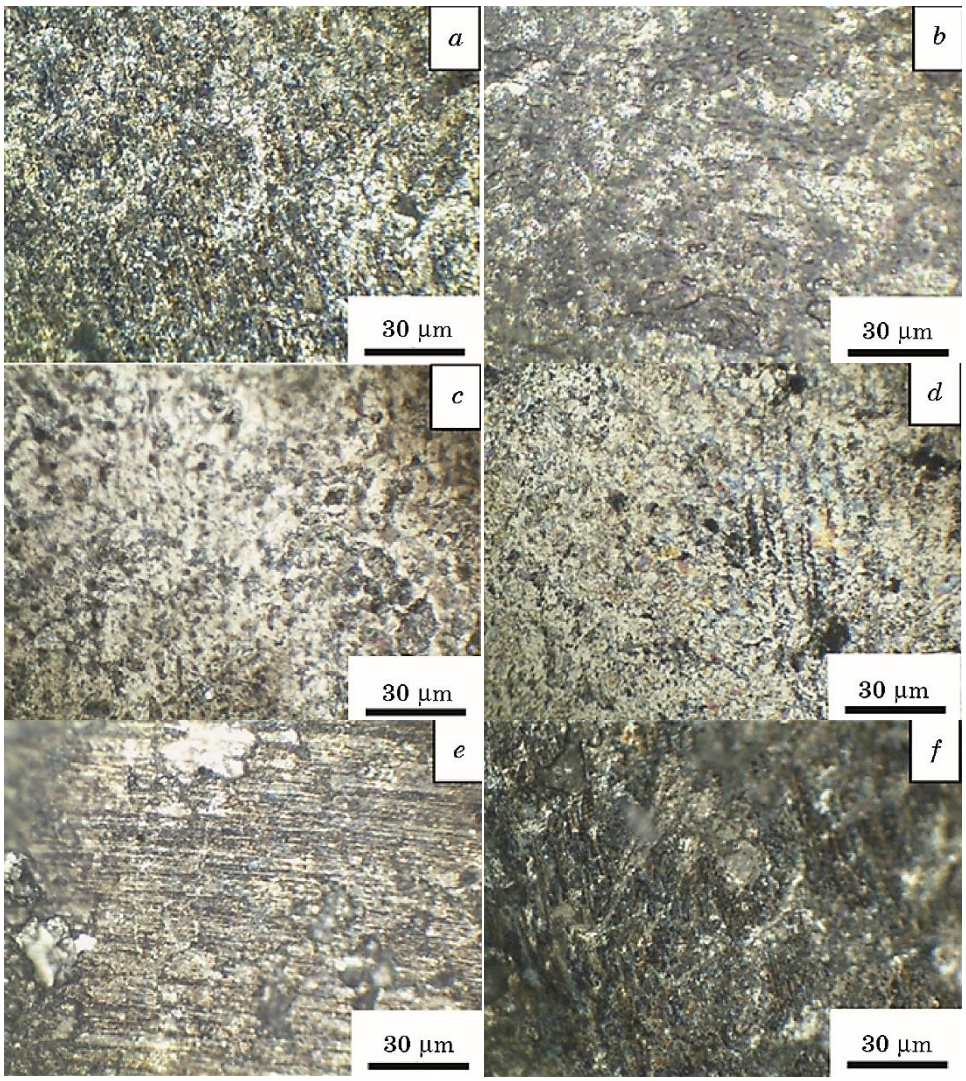


Fig. 5. Surface morphology of AISI 316 stainless steel produced by selective laser melting (*a*, *c*, *e*) and hot rolling (*b*, *d*, *f*) after heat treatment and UIT with duration that provides the maximum microhardness (Fig. 4): T0 + UIT (*a*, *b*), annealing, T1 + UIT (*c*, *d*), water quenching, T2 + UIT (*e*, *f*).

rolled AISI 316 steel in the as-received state and after heat treatment, with all specimens shown after the UIT duration that produced the maximum increase in microhardness.

The SLM specimens have a specific highly dispersed initial structure, including submicron solidification cells and remnants of the melt-track boundaries, which respond differently to deformation de-

pending on the heat treatment. In the T0 + UIT condition, a very fine, heterogeneous surface morphology is observed. The high initial defect density after 3*D* printing restricts dislocation motion. Thus, the deformation relief after UIT is strongly fragmented and rough, without pronounced linear features. T1 annealing partly relieves internal stresses and homogenizes the structure. After T1 + UIT, the surface appears more uniformly deformed and exhibits somewhat larger microrelief features, suggesting a more extensive plastic flow during UIT. After T2 + UIT, a fundamental change in morphology is observed. A directional texture with numerous parallel deformation traces (slip bands) is clearly visible on the surface. Water quenching brings the steel to a highly plastic austenitic state, allowing the metal to deform intensively under the impacts of the UIT striker and to form a pronounced textured relief.

The conventionally deformed metal is characterized by a more macroscopically homogeneous initial structure and different grain morphology. In the T0 + UIT condition, the surface appears as a heavily work-hardened rolled structure. Ultrasonic treatment produces a chaotic fine-grained relief caused by superposition of UIT-induced plastic deformation of the matrix already deformed by rolling. After T1 annealing, recrystallization occurs and the hardening induced by rolling is removed. Subsequent UIT of this stress-relieved surface forms a relatively uniform, smooth microrelief with distinct boundaries of local plastic-deformation regions. The quenched rolled steel surface after UIT shows pronounced structural fragmentation. Visually, it appears the darkest and most finely dispersed, indicating formation of an ultrafine or nanostructured sublattice in the near-surface layer because of a high degree of deformation of quenched austenite.

Figure 6 presents the XRD analysis results. The fragments of the XRD patterns (Fig. 6, *a*, *b*) contain typical reflections from austenite γ-Fe(111), martensite α′-Fe(110) and γ-Fe(200). After UIT, the intensity of the α′-Fe(110) peak gradually increases, especially for the hot-rolled material, indicating development of the $\gamma \rightarrow \alpha'$ deformation-induced martensitic transformation under cyclic impact loading. For the SLM specimens, the changes in the peak intensity are less pronounced, signalizing a higher stability of the austenitic structure.

For the SLM material (Fig. 6, *c*), the CSD size gradually decreases from ≅ 32 nm and ≅ 22 nm for γ-Fe and α′-Fe, respectively, to 12 nm and 6 nm. For the hot-rolled material (Fig. 6, *d*), the CSD size of the γ-phase decreases from 17 to 12 nm during the initial stages of treatment and then increases to 30 nm with increasing treatment duration. The CSD size of the α′-phase remains nearly unchanged up to 180 s before also increasing to approximately 30 nm. These changes reflect the evolution of the coherently diffracting domain structure during UIT and are consistent with the accumulation of lattice defects at the initial treat-

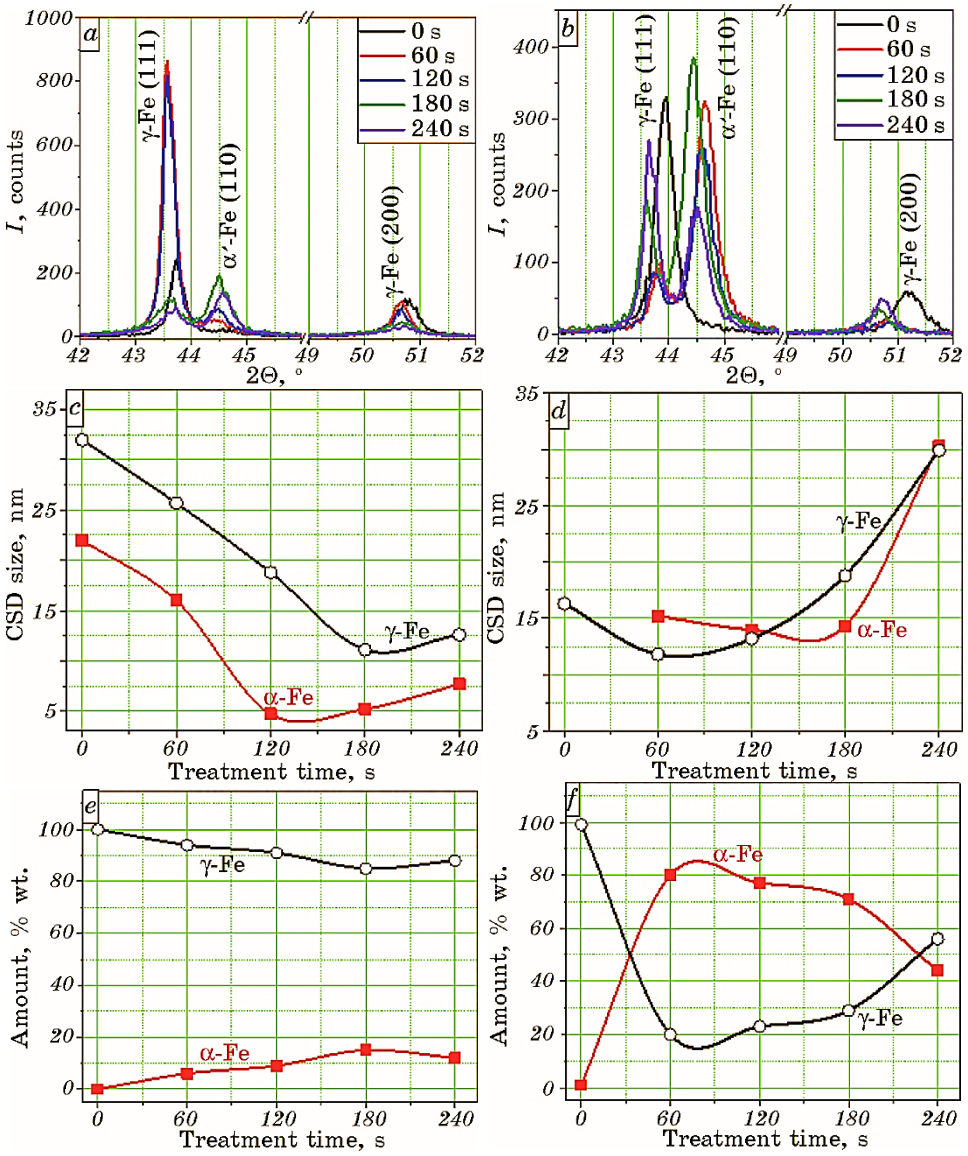


Fig. 6. Fragments of XRD patterns (*a*, *b*), CSD size (*c*, *d*), and quantitative phase composition (*e*, *f*) as a function of ultrasonic impact treatment of AISI 316 stainless steel produced by selective laser melting (*a*, *c*, *e*) and hot rolling (*b*, *d*, *f*).

ment stages, followed by their rearrangement during continued deformation.

For the SLM material (Fig. 6, *e*), the austenitic phase remains domi-

nant throughout the treatment cycle; its content decreases only from 99 to 82%. A different behaviour is observed for the hot-rolled material (Fig. 6, *f*). After only 60 s of UIT, the γ-phase fraction decreases sharply from 99% in the initial state to 20%. The phase composition then stabilizes, indicating considerably lower austenite stability after hot rolling and a high susceptibility to deformation-induced martensitic transformation.

For the SLM material (Fig. 7), the level of compressive residual stresses rapidly increases after UIT. The maximum value is reached after 60 s and is approximately –250 MPa. Subsequently, the stresses gradually relax to about –88 MPa after 240 s. In the hot-rolled material (Fig. 7), the initial state is characterized by tensile stresses; UIT produces compressive stresses in the surface layer after 180 s of treatment at a level of –100 GPa.

Formation of compressive stresses is accompanied by intensive martensitic transformation and strengthening of the surface layer.

These results agree well with the microhardness measurements. For the SLM specimens, the increase in microhardness after UIT is mainly associated with accumulation of compressive residual stresses and dislocation strengthening, while the contribution of martensitic transformation remains limited due to the high austenite stability. For the hot-rolled material, the dominant strengthening mechanism is the in-

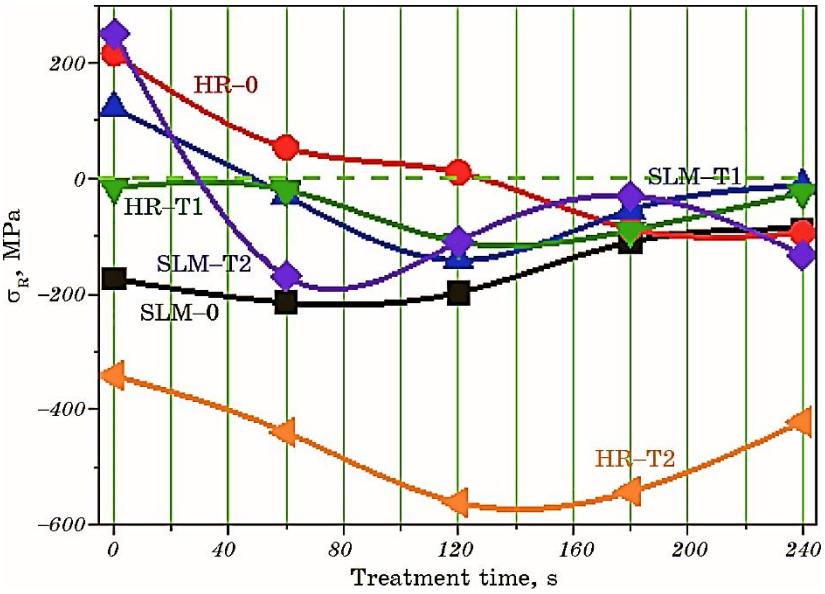


Fig. 7. Residual stress evolution as a function of ultrasonic impact treatment duration for AISI 316 stainless steel produced by selective laser melting and hot rolling.

tensive $\gamma \rightarrow \alpha'$ deformation-induced transformation, accompanied by a sharp increase in the martensite fraction and formation of compressive stresses. This is why the structural and microhardness changes after UIT are much more pronounced for the hot-rolled material compared to the AISI 316 stainless steel produced by selective laser melting.

Figure 8 shows XRD patterns, calculated changes in quantitative phase composition, coherent scattering domain size and first-order stresses for AISI 316 stainless steel produced by SLM and HR after annealing and subsequent ultrasonic impact treatment. The XRD patterns (Fig. 8, *a*, *b*) reveal diffraction peaks corresponding to austenite γ-Fe(111) and (200), as well as deformation-induced martensite α′-Fe(110). With increasing UIT duration, the intensity of the α′-Fe reflections gradually increases, suggesting the progressive $\gamma \rightarrow \alpha'$ deformation-induced martensitic transformation. Simultaneously, diffraction peak broadening is observed, indicating a reduction in the size of coherently diffracting domains and/or an increase in lattice mi-

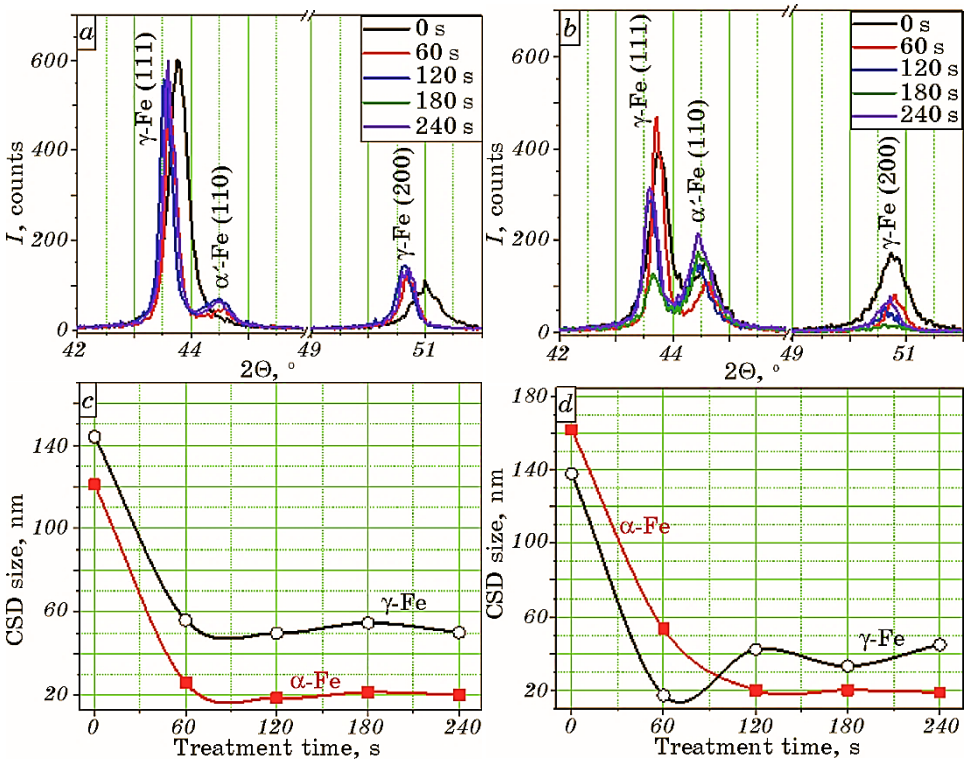
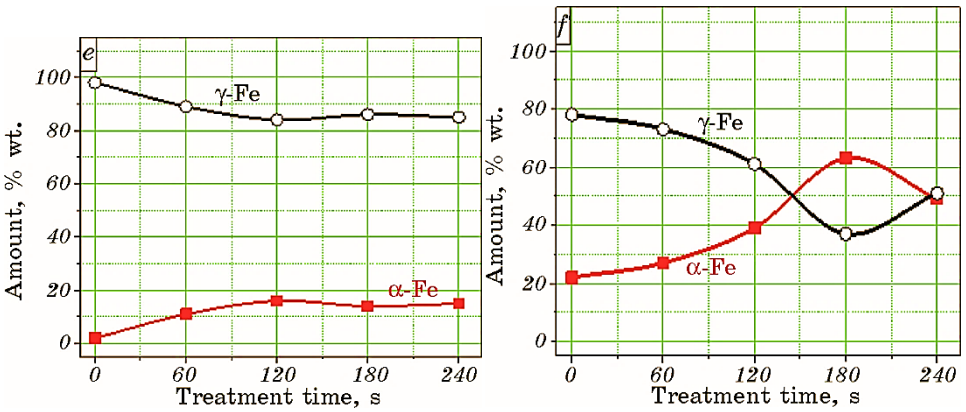


Fig. 8. Fragments of XRD patterns (*a*, *b*), change in CSD size (*c*, *d*), and change in quantitative phase composition (*e*, *f*) in AISI 316 stainless steel produced by selective laser melting (*a*, *c*, *e*) and hot rolling (*b*, *d*, *f*) after annealing (T1) and ultrasonic impact treatment.



Continuation of Fig. 8.

crostrain associated with plastic deformation of the surface layer.

For SLM AISI 316 steel (Fig. 8, *c*), the CSD size of the austenitic γ-Fe phase sharply decreases from ≅ 145 nm in the initial state to 55 nm after only 60 s of UIT. Further increase in treatment duration does not cause additional CSD refinement. For α′-martensite in the initial state, a somewhat smaller CSD size of ≅ 125 nm is observed; after UIT during 60 s, as for γ-Fe, the CSD size also sharply decreases.

For HR AISI 316 steel (Fig. 8, *d*), the CSD-size variation at the initial deformation stages is similar: the CSD sizes of γ-Fe and α′-Fe decrease sharply from 140 nm and 162 nm in the initial state to 18 nm and 58 nm after 60 s of UIT. Increasing the UIT duration leads to a gradual increase in the γ-Fe CSD size to 40 nm, whereas the α′-Fe CSD size continues to decrease and remains at ≅ 20 nm after 120 s of the treatment.

The quantitative phase analysis results (Fig. 8, *e*, *f*) show a gradual decrease in the γ-phase fraction and a corresponding increase in the α′-martensite content with increasing UIT duration for both fabrication routes of AISI 316 stainless steel.

For the SLM specimens (Fig. 8, *e*), the austenite content decreases from ≅ 95% to ≅ 80%, while for the HR material (Fig. 8, *f*) α′-phase formation is much more intensive: the γ-phase content decreases from ≅ 79% to ≅ 38% after 180 s of UIT. The higher amount of the formed α′-phase indicates a higher tendency of the rolled structure to form martensite.

The first-order residual stresses in AISI 316 stainless steel produced by selective laser melting and hot rolling after annealing and subsequent ultrasonic impact treatment are shown in Fig. 7. For the SLM steel after T1 annealing, tensile stresses of ≅ 250 MPa are registered. After UIT, compressive stresses with a maximum value of ≅ 150 MPa

are formed in the surface layer after 120 s of the treatment, followed by the partial relaxation. For HR specimens, minimum stress values are also observed near 120 s of the treatment; however, their absolute magnitude is somewhat lower ($\cong$ 120 MPa) and further treatment decreases the level of compressive stresses.

Figure 9 presents the XRD results for AISI 316 stainless steel after water quenching (HT-2) and subsequent ultrasonic impact treatment. The evolution of quantitative phase composition, CSD size, and first-order stresses as a function of deformation-treatment duration is shown.

The fragments of the XRD patterns (Fig. 9, *a*, *b*) identify (111) and (200) diffraction peaks from the austenitic γ-Fe phase and (110) peak from martensitic α′-Fe. With increasing UIT duration, the intensity of the α′-Fe(110) diffraction peak increases, indicating development of the $\gamma \rightarrow \alpha'$ deformation-induced transformation.

For SLM AISI 316 steel, the austenite to martensite transformation

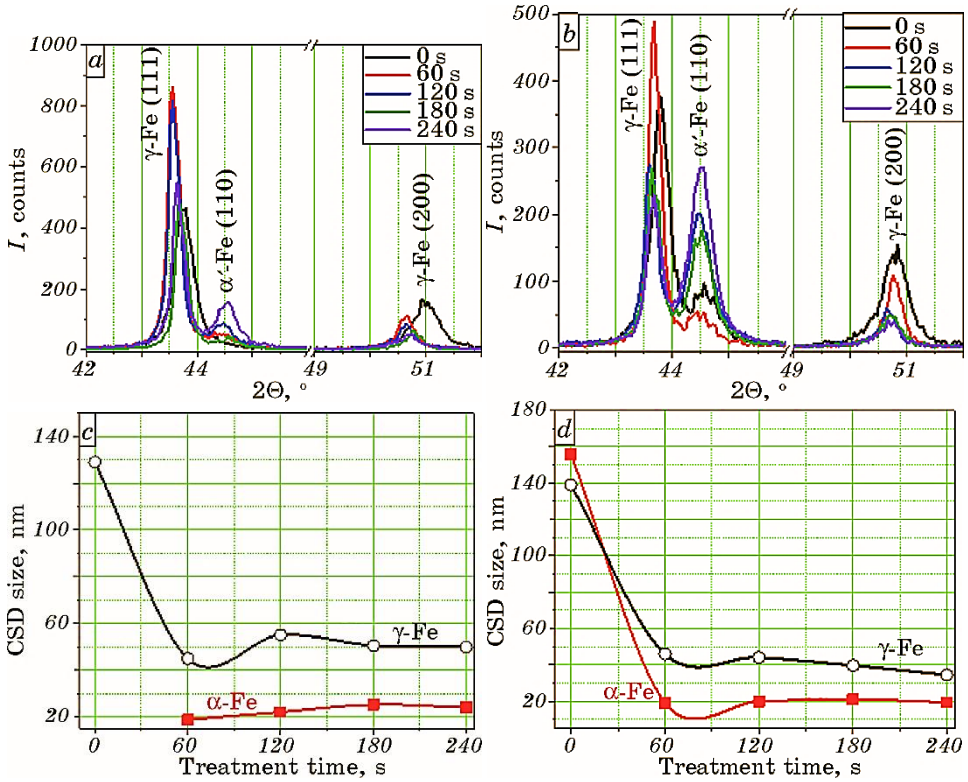
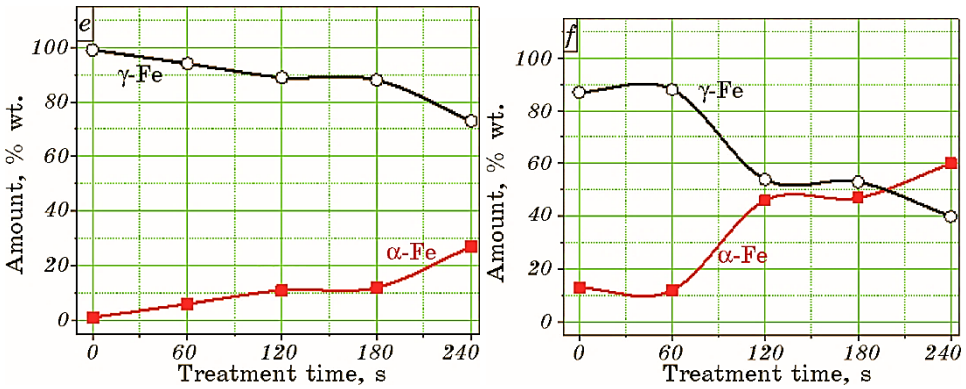


Fig. 9. Fragments of XRD patterns (*a*, *b*), change in CSD size (*c*, *d*), and change in quantitative phase composition (*e*, *f*) in AISI 316 stainless steel produced by selective laser melting (*a*, *c*, *e*) and hot rolling (*b*, *d*, *f*) after water quenching (T2) and ultrasonic impact treatment.



Continuation of Fig. 9.

occurs less intensively compared to the HR steel, indicating a lower tendency of the structure after water quenching (HT–2) to undergo martensitic transformation under deformation.

For the SLM specimen after water quenching (Fig. 9, *c*), the CSD size of austenitic γ-Fe sharply decreases from ≅ 130 nm in the initial state to 45 nm after 60 s of treatment. Further increase in treatment duration does not lead to a significant decrease in CSD size. The CSD size of α′-Fe remains substantially smaller (≅ 25 nm) and does not change with increasing treatment duration. For HR AISI 316 steel (Fig. 9, *d*), the CSD-size variation during UIT is similar.

The quantitative phase composition of AISI 316 stainless steel produced by different routes was determined from the XRD results (Fig. 9, *e*, *f*). For the both fabrication routes, after water quenching (T2) and ultrasonic impact treatment, the γ-Fe content decreases with increasing UIT duration. For the SLM specimens (Fig. 9, *e*), the γ-phase content decreases from ≅ 99% to ≅ 76% after 240 s of UIT. The process occurs gradually, indicating relatively high austenite stability after water quenching. In the hot-rolled specimens (Fig. 9, *f*), martensitic transformation is much more intensive: the γ-phase fraction decreases from 86% to 40% after 240 s of the treatment.

UIT after water quenching induces compressive residual stresses in the surface layer (Fig. 7). For the SLM specimens, tensile residual stresses of approximately 230 MPa are present after water quenching; after 60 s of UIT, they change sign and become compressive (–185 MPa). With further increasing treatment duration, the residual stress values change in a non-monotonic manner, which may be associated with local heating and stress relaxation during continued deformation. For the hot-rolled AISI 316 steel, this effect is considerably more pronounced: compressive residual stresses exceed –550 MPa after 120 s of UIT, indicating severe plastic deformation of the surface layer.

These results show that, after water quenching, subsequent ultrasonic impact treatment causes formation of deformation-induced α'-Fe martensite, reduction of the CSD size of the austenitic phase at the initial stages of UIT and accumulation of compressive residual stresses.

At the same time, SLM-produced AISI 316 steel exhibits higher austenite stability, while the HR material is characterized by more intensive martensitic transformation and formation of higher compressive stresses.

4. CONCLUSIONS

AISI 316 stainless steel produced by selective laser melting exhibited higher stability of the austenitic γ-phase during UIT, manifested by a less pronounced $\gamma \rightarrow \alpha'$ deformation-induced martensitic transformation and a different microhardness evolution compared with the hot-rolled material. This behaviour is attributed to the cellular-dendritic microstructure and residual stresses characteristic of the SLM process.

Hot-rolled specimens are characterized by a much more intensive martensitic transformation during UIT, accompanied by a substantial increase in the α'-phase fraction and formation of higher compressive residual stresses. These factors provide the maximum microhardness values after 120 s of the treatment. At the same time, after the optimal UIT duration exceeded, partial stress relaxation and phase-composition stabilization are observed; this slows slowing down the further strengthening.

Analysis of coherent scattering domain size changes showed that short-term UIT reduces the CSD size of the γ-phase, indicating refinement of the coherently diffracting domains during the initial stages of plastic deformation.

Combining water quenching with UIT increases the susceptibility of the material to deformation-induced martensitic transformation and promotes the formation of higher compressive residual stresses. This effect is more pronounced for the hot-rolled material. In SLM specimens, austenite remains more stable even after water quenching, confirming the distinct microstructural characteristics of additively manufactured AISI 316 stainless steel.

Thus, the efficiency of ultrasonic impact treatment is governed by the initial structural state of the material. Hot-rolled AISI 316 steel shows reveal more intensive deformation strengthening and martensitic transformation after UIT, whereas while the steel produced by selective laser melting is characterized by higher austenite stability and slower kinetics of changes in phase composition, microhardness and residual stresses.

This work was performed within the framework of budget-funded

project No. 2701f of Igor Sikorsky Kyiv Polytechnic Institute 'Scientific foundations of ultrasonic impact and additive technologies for manufacturing highly loaded UAV components with improved range' (No. 0124U001001).

AUTHORS' CONTRIBUTIONS

S. M. Voloshko conceived the study, contributed to the development of the research methodology, supervised the experimental work, interpreted the results, and critically revised the manuscript. I. A. Vladymyrskyi contributed to the conceptualization of the study, analysis and interpretation of the experimental results, and critical revision of the manuscript. M. I. Anyakin contributed to the preparation of the specimens, implementation of the processing procedures, and analysis of the experimental results. N. A. Shapovalova performed microstructural characterization, processed and analysed the experimental data, and contributed to the preparation of the manuscript. M. M. Voron contributed to the preparation and characterization of the investigated materials and to the analysis and interpretation of the microstructural results. A. P. Burmak designed the experimental program, performed and analysed the x-ray diffraction, microhardness, and residual-stress measurements, interpreted the obtained results, prepared the figures, and wrote the original draft of the manuscript. All authors discussed the results, contributed to the revision of the manuscript, and approved its final version.

REFERENCES

1. Z. Huang, J. Zhang, Z. Ma, S. Yuan, and H. Yang, *Appl. Sci.*, **14**, Iss. 22: 10196 (2024).
2. *Stainless Steels* (Ed. J. R. Davis) (ASM International: 1994).
3. J. Singh, V. Il'yenko, and J. P. Oliveira, *Sci. Technol. Weld. Join.*, **30**, Iss. 3: 220 (2025).
4. B. Szubzda, A. J. Antończak, P. E. Kozioł, Ł. Łazarek, B. Stępak, K. Łęcka, A. Szmaja, and M. Ozimek, *IOP Conf. Ser.: Mater. Sci. Eng.*, **113**: 012017 (2016).
5. A. S. Lima, A. M. Nascimento, H. F. G. Abreu, and P. de Lima-Neto, *J. Mater. Sci.*, **40**: 139 (2005).
6. P. Marshall, *Austenitic Stainless Steels: Microstructure and Mechanical Properties* (Springer: 1984).
7. A. Amininejad, R. Jamaati, and S. J. Hosseinipour, *Trans. Indian Inst. Metals*, **74**: 1799 (2021).
8. Y. Xiong, Y. Yue, T. He, Y. Lu, F. Ren, and W. Cao, *Materials*, **11**, Iss. 9: 1557 (2018).
9. F. K. Yan, G. Z. Liu, N. R. Tao, and K. Lu, *Acta Mater.*, **60**, Iss. 3: 1059 (2012).
10. H. A. Rezaei, M. S. Ghazani, and B. Eghbali, *Mater. Sci. Eng. A*, **736**: 364 (2018).
11. L. Zheng, H. Zang, Y. Liu, Y. Xiao, Y. Cong, Z. Cheng, G. Chen, Z. Xing, J. Pan,

Q. Jiang, W. Chen, K. Yamanouchi, H. Xu, and R. Li, *Light Sci. Appl.*, **14**: 352 (2025).
12. Y. B. Lei, Z. B. Wang, B. Zhang, Z. P. Luo, J. Lu, and K. Lu, *Acta Mater.*, **208**: 116773 (2021).
13. Z. B. Wang, J. Lu, and K. Lu, *Acta Mater.*, **53**: 2081 (2005).
14. K. Wang, N. Lin, Q. Liu, Q. Shi, Z. Liu, Q. Zeng, Y. Yu, D. Li, and Y. Wu, *J. Mater. Res. Technol.*, **38**: 5486 (2025).
15. Y. Wang, X. Shu, S. Wei, C. Liu, W. Gao, R. A. Shakoor, and R. Kahraman, *J. Alloys Compd.*, **630**: 189 (2015).
16. D. Zeng, S. Yang, and Z. D. Xiang, *Appl. Surf. Sci.*, **258**, Iss. 12: 5175 (2012).
17. J. L. Marulanda, F. J. Pérez, and A. Remolina-Millán, *J. Phys.: Conf. Ser.*, **466**: 012009 (2013).
18. E. Villabona, F. Veiga, P. J. Rivero, V. Uralde, and A. Suárez, *Steel Res. Int.*, **96**, Iss. 10: 2400976 (2025).
19. M. A. Bevan, A. A. H. Ameri, D. East, D. C. Austin, A. D. Brown, P. J. Hazell, and J. P. Escobedo-Diaz, *Characterization of Minerals, Metals, and Materials* (Eds. S. Ikhmayies, B. Li, J. S. Carpenter, J. Li, J.-Y. Hwang, S. N. Monteiro, D. Firrao, M. Zhang, Z. Peng, J. P. Escobedo-Diaz, C. Bai, Y. E. Kalay, R. Goswami, and J. Kim) (Springer: 2017), p. 577.
20. S. Behera, M. Patel, P. K. Dwivedi, R. Velayutham, A. Gaurav, and J. Murugesan, *J. Mater. Eng. Perform.*, **35**: 1873 (2026).
21. C. A. Sumanariu, C. G. Amza, F. Baciu, M. I. Vasile, and A. I. Nicoara, *Materials*, **17**, Iss. 19: 4808 (2024).
22. B. V. Efremenko, Y. G. Chabak, L. Falat, V. G. Efremenko, A. Amanov, A. M. Syrotyuk, and E. V. Tsvetkova, *Physicochem. Mech. Mater.*, **62**, Iss. 1: 17 (2026).
23. B. N. Mordyuk, G. I. Prokopenko, M. A. Vasylyev, and M. O. Iefimov, *Mater. Sci. Eng. A*, **458**, Iss. 1–2: 253 (2007).
24. B. V. Efremenko, Y. G. Chabak, A. Amanov, V. G. Efremenko, O. Milkovič, E. V. Tsvetkova, I. M. Olejnik, and A. V. Dzherenova, *J. Nano- Electron. Phys.*, **17**, No. 5: 05019 (2025).
25. *Alt-Print, 316L Data Sheet*.
26. A. P. Burmak, M. M. Voron, S. M. Voloshko, S. I. Sydorenko, I. A. Vladymyrs'kyy, S. I. Konorev, B. M. Mordyuk, and M. O. Vasyl'yev, *Metallofiz. Noveishie Tekhnol.*, **47**, No. 8: 827 (2025).
27. S. P. Chenakin, B. M. Mordyuk, N. I. Khripta, and V. Y. Malinin, *Metallofiz. Noveishie Tekhnol.*, **45**, No. 9: 1109 (2023).
28. Y. Zhang, L. Peng, Y. Wang, and C. Ye, *Proc. CIRP*, **123**: 481 (2024).
29. V. Kumar, N. K. Kumbhar, M. D. Joshi, Y.-R. Ma, I. Singh, and S. S. Hosmani, *Mater. Sci. Technol.*, **40**, Iss. 17: 1268 (2024).
30. T. Gundgire, S. Santa-aho, T. Rautio, A. Järvenpää, and M. Vippola, *J. Mater. Process. Technol.*, **323**: 118229 (2024).
31. M. Geľatko, M. Hatala, F. Botko, and R. Vandžura, *Materials*, **17**, Iss. 10: 2270 (2024).
32. I. Morozova, C. Kehm, A. Obrosov, Y. Yang, K. U. M. Miah, E. Uludintceva, S. Fritzsche, S. Weiß, and V. Michailov, *J. Mater. Eng. Perform.*, **32**: 4295 (2023).
33. M. Geľatko, M. Hatala, F. Botko, R. Vandžura, J. Hajnyš, M. Šajgalík, and J. Török, *Materials*, **16**, Iss. 19: 6461 (2023).